

# Fluid-kinetic multiscale solver for wall-bounded turbulence

Akshay Chandran<sup>1</sup>, Praveen Kumar Kolluru<sup>1</sup>, Berni J. Alder<sup>2</sup>, Sauro Succi<sup>3</sup>,  
and Santosh Ansumali<sup>1</sup>

<sup>1</sup>Jawaharlal Nehru Centre for Advanced Scientific Research, Jakkur,  
Bengaluru 560064, India

<sup>2</sup>Lawrence Livermore National Laboratory, Livermore, CA 94550, USA

<sup>3</sup>Center for Life Nano Science @ La Sapienza, Istituto Italiano di Tecnologia,  
00161 Rome, Italy

November 19, 2025

## Abstract

We present a two-level (fluid-kinetic) coupling procedure for the simulation of wall-bounded flows at Reynolds numbers up to thousands. The method combines a kinetic Direct Simulation Monte Carlo (DSMC) treatment of the near-wall layer, with a high-order Lattice-Boltzmann (HOLB) scheme as a fluid solver in the bulk flow. Given the kinetic nature of HOLB, this coupling is expected to provide a physically accurate treatment of the near-wall instabilities which trigger the transition to turbulence above a critical threshold around  $Re_c \sim 750$ .

The coupled DSMC-HOLB solver is validated by simulating plane Poiseuille and Couette flows far from equilibrium, i.e at finite Knudsen number regimes. Based on this validation, we provide the first preliminary evidence that the combination of HOLB and DSMC permits to observe the regeneration cycles of coherent structures which arise above a critical value of the Reynolds number. This task would be hardly attainable by either of the two solvers separately; while DSMC can capture strong near-wall non-equilibrium effects, it lacks the compute power to deal with both near-wall and bulk flow at the same time. We look to HOLB to make it computationally feasible to perform such a simulation. The present two-level coupling procedure may pave the way to a new generation of fluid-kinetic simulations of wall-bounded turbulent flows, thus helping to gain deeper insights into the role of wall micro-corrugations in triggering the dynamic instabilities that drive the transition to turbulent regimes.

## 1 Introduction

The emergence of fluid turbulence from the underlying molecular dynamics provides an adamant example of the amazing complexity that can arise from the collective motion of large ensembles

of microscopic degrees of freedom. For the case of fluid turbulence, such collective motion results from the strong spacetime correlations between billions of molecules that behave “as one”. The extent of such a correlation is dictated by the separation between the relevant scales of motion, namely the molecular mean free path versus the shortest turbulent scales, known as Kolmogorov length, also known as (inner) Knudsen number.

For dilute gases, described by Boltzmann’s kinetic theory, the mean free path is  $\lambda \sim 0.1 \mu\text{m}$  at STP, while the Kolmogorov scale depends on the size of the flow and the corresponding Reynolds number. For a moderately turbulent flow in a box 1 meter in size at a Reynolds number  $Re \sim 10^4$ , the Kolmogorov length is typically  $l_k \sim 1000 \mu\text{m}$ , i.e., three-four orders of magnitude above the mean-free path. A fully resolved turbulent simulation requires mesh-spacings below the Kolmogorov length, but certainly not thousands of times shorter. As a result, molecular simulations of macroscopic hydrodynamics and turbulence are justly viewed as not only computationally unviable but also physically unnecessary. This is why, historically, turbulence has been studied almost exclusively at the level of continuum fluid mechanics.

However, the validity of a continuum treatment of the near-wall flow has been questioned by a number of authors[1, 2], mostly on account of the strong non-equilibrium effects triggered by large gradients in the near-wall region of the flow, which invalidate the very foundations of the Navier-Stokes equations as a weak-gradient asymptotic limit of Boltzmann’s kinetic theory. On the other hand, such strong non-equilibrium effects are naturally incorporated within Boltzmann’s kinetic theory, hence, at least in principle, they can be handled by DSMC simulations.

Recent arguments have shown that, due to increased computing power and more advanced software, DSMC simulations of turbulence at finite Mach number is a distinct possibility because the gap between the Kolmogorov length scale and the mean free path shrinks as the Mach number is raised, according to the so-called von Karman relation  $Re = Ma/Kn$ . This relation shows that at a given value of the Reynolds number, increasing the Mach number reflects in a corresponding increase of the Knudsen number, hence a smaller separation between the mean free path and the Kolmogorov length.

To study this effect, DSMC simulations of high Mach number turbulent flows have been conducted in the recent years<sup>[3, 4]</sup>. Although less expensive than molecular dynamics, a full DSMC simulation of wall-bounded turbulent flows still remain overly demanding and practically unviable at Reynolds numbers above a few hundreds. For instance, ref. <sup>[5, 6]</sup> simulated the decay to turbulence and minimal Couette flow (MCF) simulations at Reynolds numbers around,  $Re \sim 400$ , and a Mach number  $Ma \sim 0.3$ . These simulations delivered encouraging results but required billions of particles and millions of CPU hours on a multi-petascale HPC cluster. As a result, notwithstanding these remarkable advances, a full-domain DSMC simulation at low Mach numbers remains unfeasible for turbulent flows.

Under such a state of affairs, it becomes natural to seek hybrid strategies, coupling DSMC with continuum methods. The natural choice for the latter is a discretized solver for the Navier-Stokes equations. However, since the Navier-Stokes formulation is grounded into the low-Knudsen number approximation (weak departure from local equilibrium), a formulation closer to kinetic theory would be clearly preferable. A very appealing alternative in this respect is provided by the Lattice-Boltzmann (LB) method<sup>[7, 8, 9, 10, 11]</sup>. Even though historically LB was limited to low Mach number and low Knudsen number flows, in recent years the method has matured to handle high Mach and high Knudsen number flows<sup>[12, 13, 14, 15, 16, 17]</sup>. Since such advances require higher-order stencils as compared to the standard LB schemes, we shall generically refer to them as to HOLB.

It is therefore natural to investigate what one can gain from coupling DSMC and HOLB solvers. Several attempts to couple LB with particle-based methods have been explored in the recent past<sup>[18, 19]</sup>. However, they all employ lower-order LB models and a one-way coupling.

In this work, we introduce a two-way coupling between HOLB and DSMC and show evidence of the resulting computational gains through simulations in the laminar no-slip, transitional and turbulent regimes. Wherein the individual solvers are either computationally too expensive or are unable to capture strong non-equilibrium effects near-wall in the aforementioned regimes, the coupled solver, while still more expensive than a traditional LB solver, recovers the correct macroscopic hydrodynamics in regimes that are inaccessible to standard LB models, at a fraction of the cost of a full-domain DSMC simulation. In the current HOLB, the kinetic nature of the stress dynamics is also reliably modeled.

In the high Knudsen number range, LB suffers from the discrete nature of the model and its restricted isotropy, both significantly mitigated by employing high-order stencils. DSMC<sup>[20]</sup> remains nevertheless the method of choice in the regime of high Knudsen or high Mach number. We can therefore extend the applicability of both solvers by combining them in such a way as to use DSMC in regions where non-equilibrium effects are dominant and a HOLB model in the rest of the domain.

At variance with initial works in this area using a DSMC-Lattice Boltzmann<sup>[19]</sup> and Multi-particle collision dynamics (MPCD)-Lattice Boltzmann<sup>[18]</sup> coupling in literature which extends LB completely through the domain, we restrict the DSMC solvers exclusively to the molecular regime, namely only near the wall and the HOLB solver only in the bulk, with a handshaking buffer zone for communication between them. This gives us the flexibility of moving towards high Knudsen numbers and turbulent flow regimes where the near-wall molecular layer plays a defining role in capturing boundary non-equilibrium effects.

This is important to draw the best of both models in a computationally efficient setup. In our study, without loss of any generality, we restrict discussion to the use of a class of LB models known as crystallographic, which use a body-centered cubic (BCC) ordering of the grid points<sup>[15]</sup>. We have used a 41-velocity crystallographic model, hereby referred to as the RD3Q41 model<sup>[21]</sup>. It was shown that this model ensures higher-order isotropy against the D3Q27 model and is therefore suitable for simulations in the moderate Knudsen number regime with appropriate boundary conditions. This model was also chosen due to its ability to describe low Mach number flows and acoustics in a realistic fashion.

The schematic in Figure 1 gives a picture of the implemented coupling scheme. The buffer zone represents the region where two-way DSMC-LB and LB-DSMC communication takes place. Any micro-meso-macro coupling scheme faces issues of solving the inverse problem of lifting macroscopic variables to microscopic detailed description and the generation of smooth macroscopic fields from microscopic information. In particular, for the LB to DSMC exchange, the projection of the LB moments such as the density ( $\rho$ ), momentum density ( $\rho u_\alpha$ ), stress tensor ( $\sigma_{\alpha\beta}$ ), and the heat flux ( $q_\alpha$ ) need to be used to generate the trajectory of the particles in the DSMC simulations. Conversely, once particle trajectories are evolved over a specified time interval, one needs to generate the discrete distribution to be used in the LB simulation. The communication routine performing this task is described in Section 4.

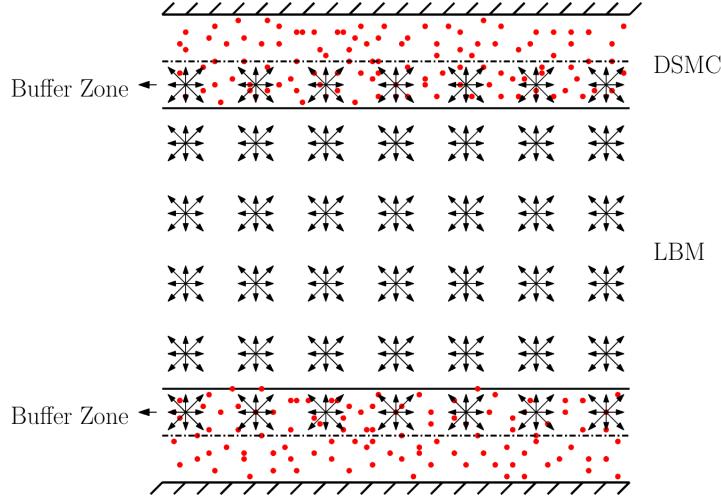


Figure 1: DSMC-HOLB coupling geometry.

## 2 Results

Finite Knudsen number flow dynamics trigger non-equilibrium effects exposing a dependence on higher-order moments beyond those needed for strictly hydrodynamic purposes. In this context, one needs to ensure that the dynamics of the higher-order moments is correct at least to the leading order, with the most critical higher-order moments being the stress ( $\sigma_{\alpha\beta}$ ), the heat flux ( $q_\alpha$ ), and the flux of heat flux ( $Q_{\alpha\beta}$ ). Thus, any LB scheme meant to match these additional moments requires extra discrete velocities<sup>[13]</sup>.

Off-grid methods like DSMC and MD do not suffer from this lack of isotropy, and wall effects can be efficiently represented in such schemes. However, as commented earlier on, such a simulation would be quite expensive. Thus, one would hope that with a DSMC layer characterizing the boundary layer, a coupled solver of DSMC paired with lattice models with high-order isotropy can dispense from the use of different boundary schemes for flows in the finite-Knudsen slip regime.

In this section, we present results for the canonical plane Poiseuille and Couette flow cases in the continuum, transitional and turbulent regimes using the multiscale method. The DSMC layer is restricted to a distance of  $\approx 4\lambda$  from either wall beyond which the LB solver covers the rest of the domain with mean temperature  $\theta_0 = 0.294896$  corresponding to the reference lattice temperature of the RD3Q41 model<sup>[21]</sup>. For these setups, the Reynolds number is  $Re = U_c L / \nu$ , based on the centerline/wall velocity  $U_c$  (corresponding to a Mach number of 0.2), full channel height  $L$  and kinematic viscosity  $\nu$  with nondimensional diffusion time defined as  $\bar{t} = t\nu/L^2$ .

In the continuum and transitional regime, the LB region has  $40 \times 40 \times 4$  lattice points and the DSMC region has  $400 \times 4 \times 40$  cells (Streamwise  $\times$  Wall-normal  $\times$  Spanwise), with  $n_0 = 100$  particles in every cell. With  $\Delta y_{LB}/\Delta y_{DSMC} = 10$ , we interpolate the moments from the first two LB nodes along the wall-normal direction and use it for particle regeneration in the LB to DSMC exchange step in a region consisting of 100 DSMC cells using Algorithm 1.

In the DSMC to LB step in the buffer layer, fluctuations arising from the DSMC region are smoothed out by spatial averaging over a region of  $5\lambda \times 5\lambda$  in the streamwise and spanwise directions and also over a timeperiod,  $t_{avg} \approx 100\tau$ , where  $\tau$  is the molecular mean free time.

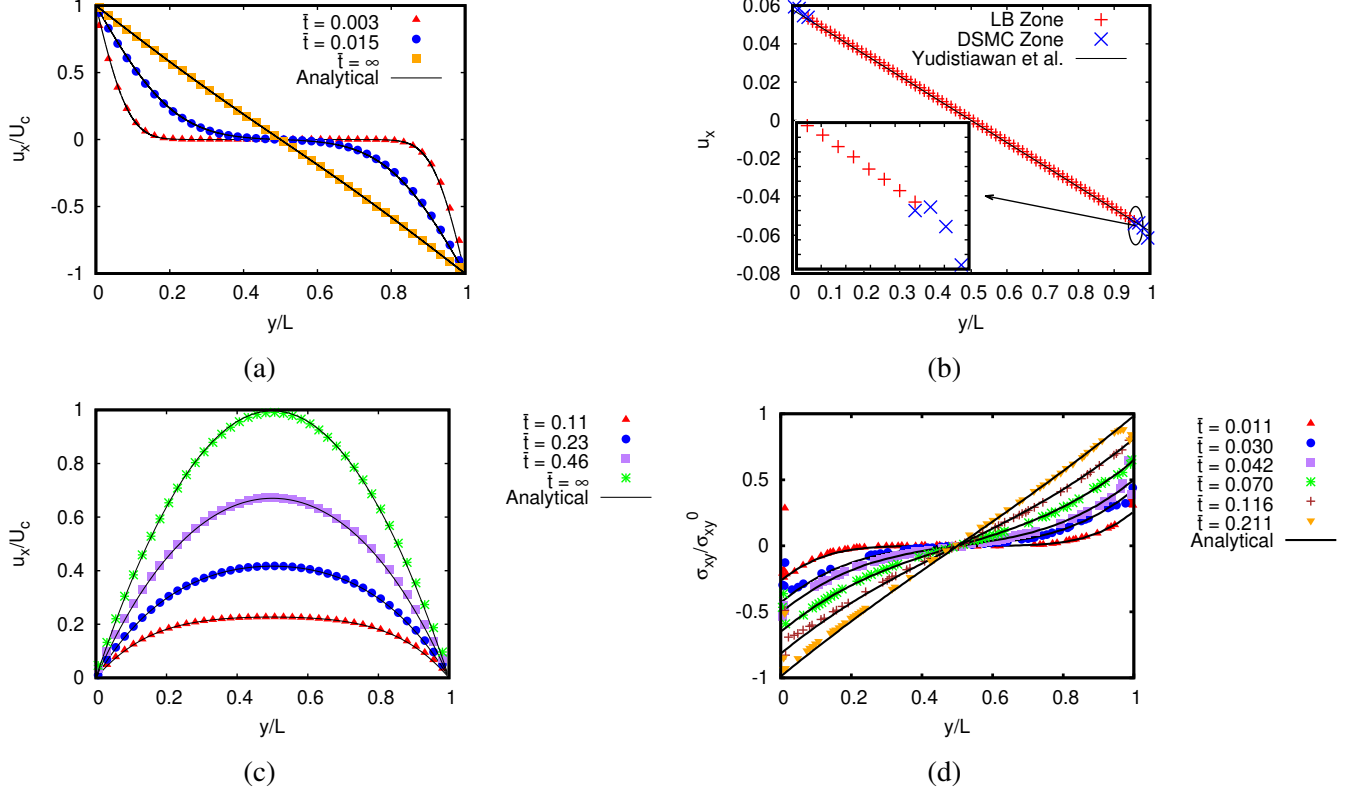


Figure 2: (a) Normalized transient velocity profile ( $u_x/U_c$ , where  $U_c$  is the wall velocity) in the continuum regime at various diffusion times compared against analytical results for a planar Couette flow at  $Re \approx 132$ ,  $Ma = 0.2$ . (b) Steady-state velocity ( $u_x$ ) profile for a Couette flow at  $Kn = 0.1$ . A zoomed-in version of the velocity profile at the upper coupling region in the inset. (c) Developing stream-wise velocity profile compared with the analytical for a plane Poiseuille flow at  $Re \approx 132$ ,  $Ma = 0.2$ . (d) Normalized transient shear stress ( $\sigma_{xy}/\sigma_{xy}^0$ ), where  $\sigma_{xy}^0$  is the wall shear stress) profile compared with the analytical solution obtained from a model kinetic equation for the same simulation.

With 128 Million particles in the wall layer, each simulation took approximately 800 CPU hours for the continuum flow and 200 CPU hours for the transitional flow on Intel<sup>®</sup> Xeon<sup>®</sup> 8,268 processors for  $\bar{t} = 1$ .

To benchmark the code, in Figure 2a, the transient velocity profiles for simulated Couette flow are contrasted with the analytical solution of the Navier-Stokes equations<sup>[22]</sup>. In order to check the accuracy at finite Knudsen number, in Figure 2b, the result from the plane Couette flow simulation at  $Kn = 0.1$  was contrasted with the steady-state velocity profile obtained from a model kinetic equation<sup>[23]</sup>. It is also evident that the overlap regions between LB and DSMC do not show any appreciable discontinuity.

As a second setup, Figure 2c contrasts the developing stream-wise velocity from our numerical simulation at  $Re \approx 132$  with the analytical profile for an acceleration driven plane channel flow in the continuum regime at any arbitrary time  $t$ <sup>[24]</sup>. Similarly, Figure 2d also contrasts the transient shear stress profile with the analytical<sup>[24]</sup> profile. With the local Mach number  $\approx 0.0087$  near the wall, the numerical value of the wall shear stress is also quite small ( $\sigma_{xy}^0$  is of  $\mathcal{O}(10^{-6})$ ), leading to significant fluctuations in the higher-order moments near the wall.

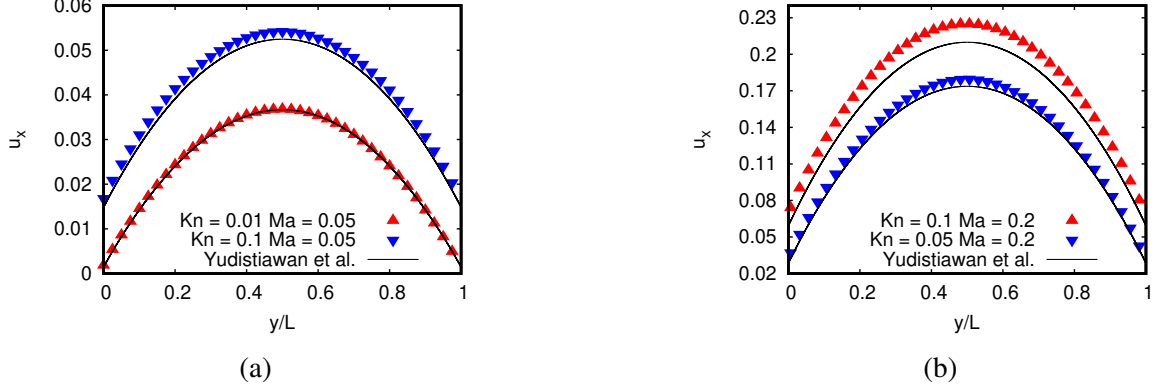


Figure 3: Steady-state velocity ( $u_x$ ) profiles for a Poiseuille flow using an LBM RD3Q41 model<sup>[21]</sup> at (a)  $Ma = 0.05$  and  $Kn = 0.01, 0.1$ , (b)  $Ma = 0.2$  and  $Kn = 0.05, 0.1$ .

The standard deviation of these fluctuations decreases with an increase in the number of particles per cell, as detailed in the supplementary material. The beneficial effects of increasing  $N$  in taming statistical fluctuations is apparent, although their decay does not seem to obey a uniform  $1/\sqrt{N}$  decay in space, which is in line with the non-equilibrium nature of the phenomenon in point.

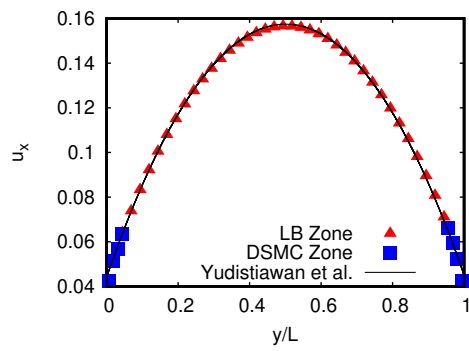
Limitations arising at finite Knudsen numbers in the lattice boltzmann method can be seen in Figures 3a & 3b, wherein at progressively higher Mach and Knudsen numbers, the deviations from ref.[23] show an increase. Using the coupled scheme, Figure 4a & 4b compares the steady-state velocity and shear stress profiles against their analytical solutions at  $Kn = 0.1$ . Here the higher-order moment,  $\sigma_{xy}$  shows a good match with the numerically approximate value. Higher-order moments ( $\sigma_{xx}, \sigma_{yy}, \sigma_{zz}$ ) as shown in Figure 4d show a smooth transition in the coupling region, with deviations in the DSMC region against the bulk arising at  $\mathcal{O}(10^{-6})$ . Meanwhile, in Figure 4c the temperature profile shows the relative cooling of the bulk as compared to the walls.

## 2.1 Turbulent plane Couette flow

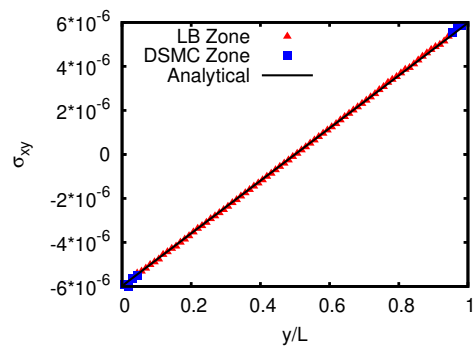
A turbulent simulation was performed for a Minimal Couette flow (MCF) setup with the bulk LB region consisting of  $720 \times 200 \times 400$  nodes and each DSMC region consisting of  $720 \times 4 \times 1200$  cells and  $n_0 = 200$  particles per cell (approximate memory requirement of 100 GB for the DSMC regions with about 1.4 billion particles). The solver took 120 hours using 2400 cores on Intel<sup>®</sup> Xeon<sup>®</sup> 8268 processors to reach 30 convection times ( $L/U_c$ ). Beyond which averaging was done over another 10 convection times.

At the fully developed state, the velocity profile in plane Couette flow is monotonic in the laminar and turbulent regimes. While linear stability theory predicts that two-dimensional disturbances are damped for plane Couette and pipe flows<sup>[25, 26]</sup>, experiments have shown that for large enough initial disturbances, the flow transitions to turbulence subcritically<sup>[27, 28, 29]</sup>. Experimental<sup>[30]</sup> and numerical<sup>[31]</sup> studies performed to determine the transitional  $Re$  have shown excellent agreement, with the former predicting the critical threshold at  $720 \pm 20$ , while the latter at 750.

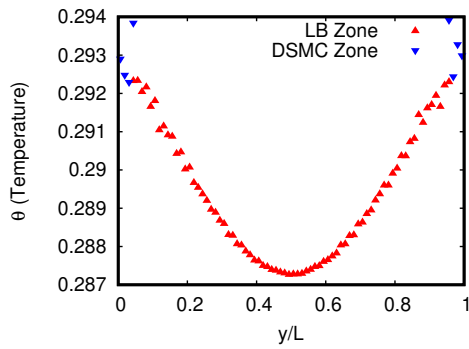
When the initial flow field is disturbed using a finite-amplitude perturbation, plane Couette



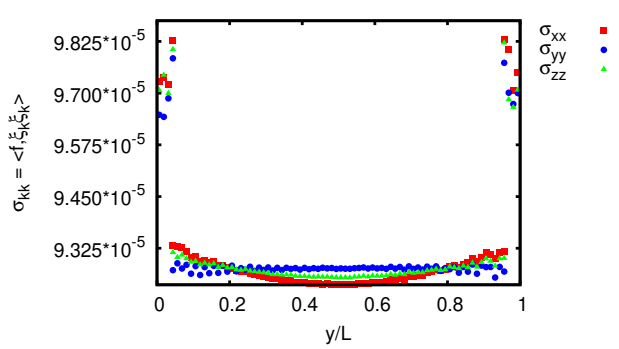
(a)



(b)



(c)



(d)

Figure 4: Steady-state (a) velocity ( $u_x$ ) and (b) Shear stress ( $\sigma_{xy}$ ) profiles for a Poiseuille flow at  $Kn = 0.1$ . Steady-state (c) temperature ( $\theta$ ) and (d) stress tensor components ( $\sigma_{xx}$ ,  $\sigma_{yy}$ ,  $\sigma_{zz}$ ) profiles for a poiseuille flow at  $Kn = 0.1$ .

flow transitions at  $Re \approx 750$ . Thousands of experimental and numerical studies performed on pipe flow have shown that the turbulent state in such linearly stable shear flows belongs to a transient turbulent chaotic saddle<sup>[32]</sup>. The implication of this is that rather than a critical  $Re$  beyond which turbulence is believed to self-sustain indefinitely, there exists a time scale  $\tau(Re)$  defining the lifetime of a turbulent state. More precisely, the probability distribution of lifetimes increases exponentially with the Reynolds number but stays finite, meaning that with long enough observation times, all linearly stable shear flows are seen to decay and relaminarize<sup>[32]</sup>. Similar observations apply to plane Couette flows<sup>[33]</sup>.

For a Couette flow, following an exponential scaling of lifetime with  $Re$ , we get a lifetime of  $\mathcal{O}(10^{24})$  convection times at  $Re = 1300$ , far longer than with any foreseeable numerical and experimental capabilities.

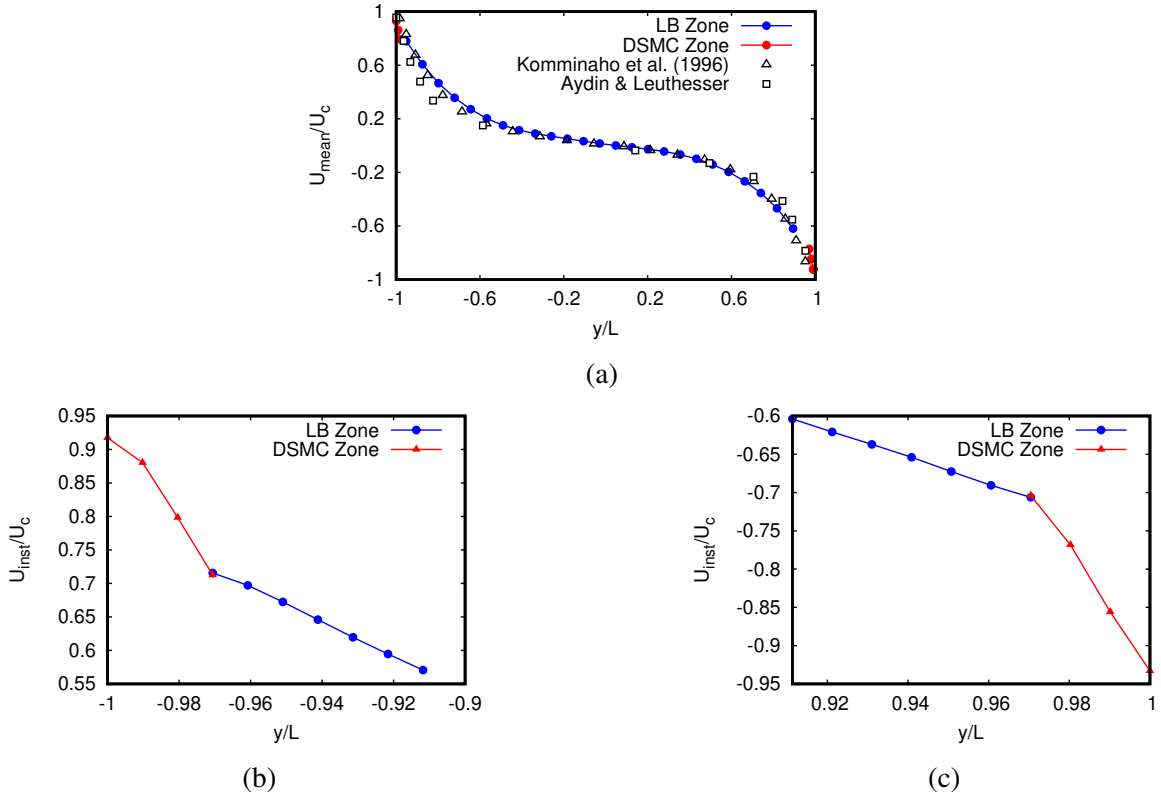


Figure 5: (a) Turbulent steady-state mean velocity profile from the coupled solver compared against the numerical profile from [34] and experimental profile from ref.[35]. Here,  $U_c$  represents the imparted wall velocity. (b) & (c) A zoomed-in version of the lower (left) and upper (right) coupling interface in the instantaneous stream-wise velocity profile.

The role of thermal fluctuations was recently shown through DSMC and NS simulations where the former predicts a quadratic growth while the latter an exponential decay of the sub-kolmogorov energy spectra<sup>[36]</sup>. On the same note, the influence of the wall micro-roughness on the transition process is an important and still pending item. Using a coupled solver with the DSMC layer provides a suitable and alternative boundary condition to the micro-roughness of the wall, and consequently, it can help in gaining deeper insights into this fundamental problem. Similarly, the transition Reynolds number for highly compressible flows is also unknown, hence the present simulations of turbulent plane Couette flow provide an initial step to explore this

important question.

Turbulent flow simulations of MCF at Reynolds number of  $Re \approx 1318$  were performed using the present coupled method. Similar simulations with standard LB solver relaminarizes after a few convection times. The coupled solver in this case helps in capturing the slow regeneration cycles in turbulent MCF. The domain was initially disturbed using a finite-amplitude perturbation generated using a curl-based Perlin noise<sup>[37]</sup>.

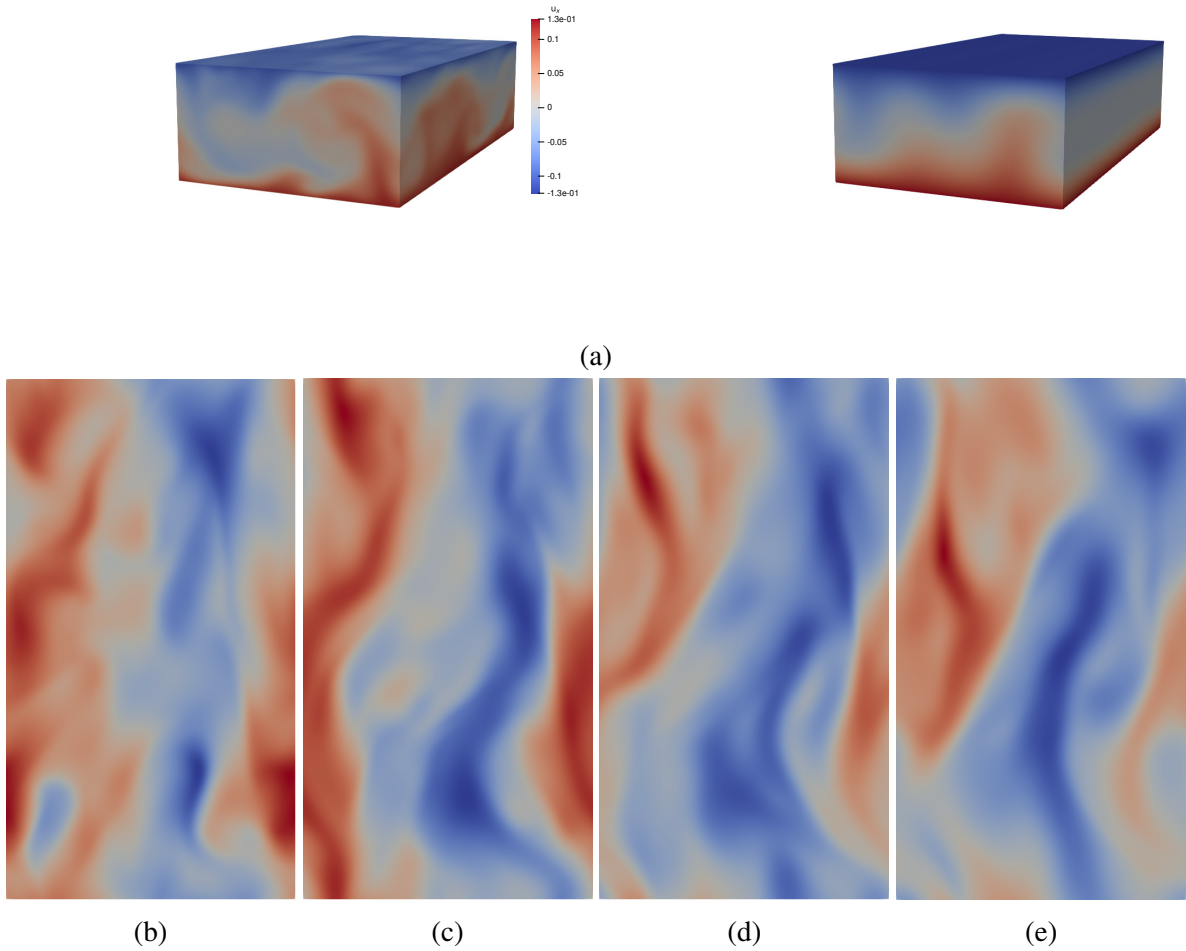


Figure 6: (a) Streamwise velocity ( $u_x$ ) field for a DSMC-LB coupled Minimal Turbulent Couette flow (taken after 20 convection times) compared against an LB simulation with the same parameters. (b)-(e) Cycle of Regeneration and decay of coherent structures in Minimal Couette flow at the channel mid-plane. Snapshots were taken at 14, 20, 22, and 25 convection times respectively.

Figure 5a compares the mean velocity obtained after spatial averaging along the spanwise and stream-wise directions as well as time averaging over 10 convection times. The numerical profile from ref.[34] have performed an averaging over 620 convection times. As there is constant decay and regeneration in the near-wall region in turbulent Couette flow, an averaging over a timescale larger than the regeneration time scale would be required. We still observe

a good agreement between the DSMC-LB coupled solver and the profiles from ref.[34] and ref.[35] near the channel mid-plane. The deviations near the wall result due to the noise from the DSMC solver in the region. We performed similar simulations using  $n_0 = 30$  to 100 and observed the averaged velocity profile to deviate further as we lower the number of particles per cell. In Figures 5b & 5c, we show the coupling interface using the instantaneous stream-wise velocity profile.

Figure 6a presents a visualization of the streamwise velocity ( $u_x$ ) field taken after 20 convection times and is compared against a corresponding LB simulation run using the same parameters. One can see the presence of coherent structures in both simulations. The LB velocity profile is smoother as compared to its DSMC-HOLB counterpart and results in the HOLB simulation to relaminarize after about fifty convection times. For linearly stable flows, finite lifetimes have been observed in similar studies on pipe flows<sup>[32]</sup>. A further perturbation to the relaminarized state leads to the cycles of regeneration and decay. As the DSMC layer injects thermal noise into the bulk LB, such a relaminarization could take longer to achieve.

Figure 6b-e shows the streamwise velocity contours at the channel mid-plane taken at various convection times. We see long coherent structures that undergo cycles of regeneration and decay indicating the sustenance of turbulence using the coupled solver. As observed in similar studies<sup>[5]</sup>, we observe two vortices that occupy half the spanwise width with anti-parallel orientation along the streamwise direction. Where ref. [5] performed full-domain DSMC simulations using almost 600 million CPU hours, our coupled solver has achieved a similar feat, yet on a smaller scale, using 0.3 million CPU hours. Although full-domain LB simulations take significantly lower time, to study the effect of sustained turbulence, relaminarization in LB simulations are a hurdle, as one needs to provide frequent disturbances to the LB simulation in order to sustain turbulence. Therefore, the coupled DSMC-LB solver can be used to study the effects of turbulence in linearly stable shear flows, at an affordable computational cost while providing accuracy comparable with microscopic simulations<sup>[5]</sup>.

### 3 Discussion

In this work, a kinetic-continuum approach using DSMC and high-order LB<sup>[21]</sup> was developed.

The coupling was tested in the continuum, transitional and turbulent regimes to validate the coupled solver. All simulations were performed using the channel flow geometry with a DSMC wall layer and an LB region in the bulk. In the continuum regime, test cases were performed on the canonical plane Couette and Poiseuille flows at  $Re = \mathcal{O}(10^2)$  and  $Ma = 0.2$  and the corresponding results served as a benchmark to show the ability and efficiency of the coupled solver in reproducing Navier-Stokes hydrodynamics with higher-order moments in good agreement with theory.

A set of simulations were then performed on canonical cases in the transitional regime to demonstrate the smooth transition of moments across the coupling region, with deviations arising only at  $\mathcal{O}(10^{-6})$  after sufficient statistical averaging.

Finally, first-time turbulent flow simulations using the coupled solver were performed for the Minimal Turbulent Couette flow at  $Re \approx 1318$  and  $Ma = 0.2$ . We observe the decay and regeneration cycles at small time scales and the characteristic S-shape of the flow is reproduced and validated against experimental and numerical simulations. Future work using the coupled solver will focus on assessing transition thresholds in turbulent plane Poiseuille flows. With

the inherent thermal noise from the DSMC wall layer, artificial forcing to transition Poiseuille flows may become redundant, and work along these lines is currently in progress. Other areas of focus are systems with high thermal gradients where local Mach numbers exceed the standard LB limits.

To summarize, our results point towards Bernie Alder’s early hunch, namely that the revival of turbulence cannot be modeled by the Navier-Stokes equations because continuum fluid mechanics fails to account for the strong non-equilibrium effects that arise in the near-wall region. A similar statement would also apply to standard hydrodynamic LB methods. High-order LB are better positioned because they can accommodate mild non-equilibrium effects, but still, this is not sufficient for quantitative purposes, unless they are coupled to a DSMC treatment of the boundary layer. An appealing possibility for the future is to replace DSMC with a stochastic near-wall forcing term in the HOLB formulation. However, the multiscale LB-DSMC procedure presented in this work is physically more sound and arguably also more robust from the numerical standpoint.

## 4 Methods

**Particle regeneration algorithm.** Particle generation follows a Monte-Carlo sampling procedure akin to ref.[38].

---

### Algorithm 1 Particle Regeneration

---

- 1: **while**  $N_i \leq N_{\text{bufferCells}}$  **do**
  - 2:      $n_{\text{poisson}} = \text{poissonDist}(\rho_{\text{LB}} V_c)$
  - 3:     **while**  $n_0 \leq n_{\text{poisson}}$  **do**
  - 4:         Compute maxima of the coefficients of the Hermite polynomials
 
$$C = \max(|a_{\text{LB}}^{(0)}|, |a_{\text{LB},\alpha}^{(1)}|, |a_{\text{LB},\beta\gamma}^{(2)}|, |a_{\text{LB},\kappa}^{(3)}|)$$
  - 5:         Generate<sup>[39]</sup> random particle velocities  $\xi$  from the Maxwell-Boltzmann distribution with temperature  $\theta_{\text{LB}}$
  - 6:         Select  $\xi$  **if**  $C\mathcal{R} \leq f(\mathbf{x}, \xi, t)$ , where  $\mathcal{R} \in (0,1)$ ; **else goto** step 5
  - 7:         Compute particle velocity using  $c_\alpha = \xi_\alpha + u_{\text{LB},\alpha}$
  - 8:     **end while**
  - 9: **end while**
  - 10: rescale all  $c_\alpha$  within cell to match  $u_{\text{LB},\alpha}$  and  $\theta_{\text{LB}}$
- 

**DSMC-LBM coupling scheme.** The first ingredient to set up the coupling between the two methods is establishing an information-exchange protocol between the two. This is naturally provided by Grad’s moment method, which consists of a systematic expansion of the Boltzmann distribution onto a suitable set of basis functions in velocity space, typically tensor Hermite polynomials. In other words, Grad’s moment method provide a natural way to lift extended list of macroscopic variables to microscopic description of distribution functions<sup>[40]</sup>.

The distribution function  $f(\mathbf{x}, \xi, t)$  is expanded in terms of Hermite orthonormal polynomial

of the peculiar velocity  $\boldsymbol{\xi} = \mathbf{c} - \mathbf{u}$  as

$$f(\mathbf{x}, \boldsymbol{\xi}, t) = w(\boldsymbol{\xi}) \sum_{n=0}^N \mathbf{a}^{(n)}(\mathbf{x}, t) \mathcal{H}^{(n)}(\boldsymbol{\xi}), \quad (1)$$

where order  $N$  is pre-specified and  $\mathcal{H}^{(n)}(\boldsymbol{\xi})$  are the Hermite polynomials at  $n^{\text{th}}$  order,  $\mathbf{a}^{(n)}(\mathbf{x}, t)$  are their corresponding coefficients,  $w(\boldsymbol{\xi})$  is the Maxwell-Boltzmann distribution at reference condition for the various Hermite polynomials<sup>[40]</sup>.

We achieve macro-micro communication through the generation of a 13-moments Grad-distribution function in explicit form as follows:<sup>[40]</sup>

$$f(\mathbf{x}, \boldsymbol{\xi}, t) = F^{\text{grad}}(\mathbf{x}, \boldsymbol{\xi}, t) = w(\boldsymbol{\xi}) \left[ \rho + \frac{\sigma_{\beta\gamma}}{2\theta_0^2} (\xi_\beta \xi_\gamma - \theta_0 \delta_{\beta\gamma}) + \frac{q_\kappa}{5\theta_0^3} (\xi^2 \xi_\kappa - 5\theta_0 \xi_\kappa) \right]. \quad (2)$$

Once Grad's distribution function is formed, particle positions and velocities can be generated using a Monte-Carlo sampling. The procedure for converting from this non-equilibrium distribution to the individual particle velocities is outlined in Algorithm 1.

In the LB framework, one uses the discrete form of the Hermite expansion<sup>[41]</sup> where the weights ( $w_i$ ) associated with the discrete velocity set are used in place of the discrete equilibrium function. Through a similar process of Gram-Schmidt orthonormalization and discrete orthonormality condition, we obtain the discrete Hermite polynomials and their coefficients<sup>[42]</sup>. Using these coefficients, one writes down the discrete Grad-distribution function as a weighted sum of discrete Hermite polynomials:

$$f_i = w_i \left[ \rho + \frac{j_\alpha c_{i\alpha}}{\theta_0} + \frac{(P_{\beta\gamma} - \rho \theta_0 \delta_{\beta\gamma})}{2\theta_0^2} (c_{i\beta} c_{i\gamma} - \theta_0 \delta_{\beta\gamma}) + \frac{(Q_\kappa - 5j_\kappa \theta_0)}{10\theta_0^3} (c_i^2 c_{i\kappa} - 5\theta_0 c_{i\kappa}) \right]. \quad (3)$$

For the DSMC to LB coupling, the moments from the DSMC region are spatially averaged over a region extending far beyond the DSMC cell dimension. This is to ensure that the discrete equilibrium in the corresponding LB nodes in the buffer layer remain positive. Here, the moments ( $\rho, j_\alpha, P_{\alpha\beta}, Q_\kappa$ ) in Equation (3) are spatially and temporally averaged from the DSMC cells in the buffer layer.

The steps followed for a single iteration of the coupling algorithm are as follows:

1. DSMC advection and collision for  $n$  ( $= \Delta t_{\text{LB}} / \Delta t_{\text{DSMC}}$ ) steps.
2. DSMC to LB moment exchange in the buffer layer through the discrete Grad distribution function (Equation (3)) followed by LB streaming and collision.
3. LB to DSMC moment exchange in the buffer layer with particle velocity regeneration using a Monte-Carlo sampling procedure (Algorithm 1).

Algorithm 2 provides a pseudo code for clarity.

### Acknowledgements

The support and the resources provided by the 'PARAM Yukti Facility' under the National Supercomputing Mission, Government of India at the Jawaharlal Nehru Centre For Advanced Scientific Research are gratefully acknowledged. One of the authors (SS) kindly acknowledges funding from the European Research Council under the Horizon 2020 Programme Grant Agreement n. 739964 ("COPMAT").

---

**Algorithm 2** Coupling methodology

---

```
1: for  $i, j \in$  DSMC region do
2:   while  $steps < n$  do
3:     advection via equations of motion
4:     particle collisions
5:     calculate moments in buffer layer
6:   end while
7: end for
8: calculate LB populations through Equation (3) in the buffer layer
9: for  $i, j \in$  LB region do
10:  advect
11:  collide
12:  calculate moments in buffer layer
13: end for
14: interpolate LB moments and regenerate particles using Algorithm 1
15: goto top
```

---

## References

- [1] Duncan A Lockerby, Jason M Reese, and Michael A Gallis. The usefulness of higher-order constitutive relations for describing the knudsen layer. *Physics of Fluids*, 17(10):100609, 2005.
- [2] Maurice N Kogan. *Rarefied gas dynamics*. Springer, 2013.
- [3] Sahadev Pradhan and V Kumaran. Transition and turbulence in a wall-bounded channel flow at high mach number. In *52nd AIAA/SAE/ASEE Joint Propulsion Conference*, page 5050, 2016.
- [4] MA Gallis, JR Torczynski, MC Krygier, NP Bitter, and SJ Plimpton. Turbulence at the edge of continuum. *Physical Review Fluids*, 6(1):013401, 2021.
- [5] Michail A Gallis, John R Torczynski, Neal P Bitter, Timothy P Koehler, Steven J Plimpton, and George Papadakis. Gas-kinetic simulation of sustained turbulence in minimal couette flow. *Physical Review Fluids*, 3(7):071402, 2018.
- [6] MA Gallis, NP Bitter, TP Koehler, JR Torczynski, SJ Plimpton, and G Papadakis. Molecular-level simulations of turbulence and its decay. *Physical Review Letters*, 118(6):064501, 2017.
- [7] Sauro Succi. *The lattice Boltzmann equation: for fluid dynamics and beyond*. Oxford university press, 2001.
- [8] Shiyi Chen and Gary D Doolen. Lattice boltzmann method for fluid flows. *Annual review of fluid mechanics*, 30(1):329–364, 1998.
- [9] Roberto Benzi, Sauro Succi, and Massimo Vergassola. The lattice boltzmann equation: theory and applications. *Physics Reports*, 222(3):145–197, 1992.

- [10] Sauro Succi and S Succi. *The lattice Boltzmann equation: for complex states of flowing matter*. Oxford University Press, 2018.
- [11] Hudong Chen, Satheesh Kandasamy, Steven Orszag, Rick Shock, Sauro Succi, and Victor Yakhot. Extended boltzmann kinetic equation for turbulent flows. *Science*, 301(5633):633–636, 2003.
- [12] R Benzi, L Biferale, M Sbragaglia, S Succi, and F Toschi. Mesoscopic two-phase model for describing apparent slip in micro-channel flows. *EPL (Europhysics Letters)*, 74(4):651, 2006.
- [13] S Ansumali, IV Karlin, S Arcidiacono, A Abbas, and NI Prasianakis. Hydrodynamics beyond navier-stokes: Exact solution to the lattice boltzmann hierarchy. *Physical review letters*, 98(12):124502, 2007.
- [14] Nicolò Frapolli, Shyam S Chikatamarla, and Iliya V Karlin. Entropic lattice boltzmann model for compressible flows. *Physical Review E*, 92(6):061301, 2015.
- [15] Manjusha Namburi, Siddharth Krithivasan, and Santosh Ansumali. Crystallographic lattice boltzmann method. *Scientific reports*, 6:27172, 2016.
- [16] Mohammad Atif, Manjusha Namburi, and Santosh Ansumali. Higher-order lattice boltzmann model for thermohydrodynamics. *Physical Review E*, 98(5):053311, 2018.
- [17] A Montessori, P Prestininzi, M La Rocca, and S Succi. Lattice boltzmann approach for complex nonequilibrium flows. *Physical Review E*, 92(4):043308, 2015.
- [18] Andrea Montessori, Adriano Tiribocchi, Marco Lauricella, Fabio Bonaccorso, and Sauro Succi. A multiresolution mesoscale approach for microscale hydrodynamics. *Advanced Theory and Simulations*, 3(4):1900250, 2020.
- [19] Gianluca Di Staso, HJH Clercx, Sauro Succi, and Federico Toschi. Dsmc–lbm mapping scheme for rarefied and non-rarefied gas flows. *Journal of Computational Science*, 17:357–369, 2016.
- [20] Graeme A Bird and JM Brady. *Molecular gas dynamics and the direct simulation of gas flows*, volume 5. Clarendon press Oxford, 1994.
- [21] Praveen Kumar Kolluru, Mohammad Atif, Manjusha Namburi, and Santosh Ansumali. Lattice boltzmann model for weakly compressible flows. *Physical Review E*, 101(1):013309, 2020.
- [22] L Gary Leal. *Advanced transport phenomena: fluid mechanics and convective transport processes*, volume 7. Cambridge University Press, 2007.
- [23] Wahyu Perdana Yudistiawan, Sang Kyu Kwak, DV Patil, and Santosh Ansumali. Higher-order galilean-invariant lattice boltzmann model for microflows: Single-component gas. *Physical Review E*, 82(4):046701, 2010.
- [24] Tasos Papanastasiou, Georgios Georgiou, and Andreas N Alexandrou. *Viscous fluid flow*. CRC press, 2021.

- [25] Wolfgang Wasow. On small disturbances of plane couette flow. *J. Res. Nat. Bur. Stand.*, 51(4):195–202, 1953.
- [26] AP Gallagher and A McD Mercer. On the behaviour of small disturbances in plane couette flow. *Journal of Fluid Mechanics*, 13(1):91–100, 1962.
- [27] SJ Davies and CM White. An experimental study of the flow of water in pipes of rectangular section. *Proceedings of the Royal Society of London. Series A, Containing Papers of a Mathematical and Physical Character*, 119(781):92–107, 1928.
- [28] Timothy W Kao and C Park. Experimental investigations of the stability of channel flows. part 1. flow of a single liquid in a rectangular channel. *Journal of Fluid Mechanics*, 43(1):145–164, 1970.
- [29] VC Patel and MR Head. Some observations on skin friction and velocity profiles in fully developed pipe and channel flows. *Journal of Fluid Mechanics*, 38(1):181–201, 1969.
- [30] Nils Tillmark and P Henrik Alfredsson. Experiments on transition in plane couette flow. *Journal of Fluid Mechanics*, 235:89–102, 1992.
- [31] Anders Lundbladh and Arne V Johansson. Direct simulation of turbulent spots in plane couette flow. *Journal of Fluid Mechanics*, 229:499–516, 1991.
- [32] Björn Hof, Jerry Westerweel, Tobias M Schneider, and Bruno Eckhardt. Finite lifetime of turbulence in shear flows. *Nature*, 443(7107):59–62, 2006.
- [33] Armin Schmiegell and Bruno Eckhardt. Fractal stability border in plane couette flow. *Physical review letters*, 79(26):5250, 1997.
- [34] Jukka Komminaho, Anders Lundbladh, and Arne V Johansson. Very large structures in plane turbulent couette flow. *Journal of Fluid Mechanics*, 320:259–285, 1996.
- [35] Mahir Aydin and Hans J Leutheusser. Novel experimental facility for the study of plane couette flow. *Review of Scientific Instruments*, 50(11):1362–1366, 1979.
- [36] John R. Torczynski Ryan M. McMullen, Michael C. Krygier and Michael A. Gallis. Navier-stokes equations do not describe the smallest scales of turbulence in gases. *Physical Review Letters*, 128(11):114501, 2022.
- [37] Robert Bridson, Jim Houriham, and Marcus Nordenstam. Curl-noise for procedural fluid flow. *ACM Transactions on Graphics (ToG)*, 26(3):46–es, 2007.
- [38] Alejandro L Garcia and Berni J Alder. Generation of the chapman–enskog distribution. *Journal of computational physics*, 140(1):66–70, 1998.
- [39] Samarth Agrawal, Soumyadeep Bhattacharya, and Santosh Ansumali. Molecular dice: Random number generators á la boltzmann. *Physical Review E*, 98(6):063315, 2018.
- [40] Harold Grad. On the kinetic theory of rarefied gases. *Communications on pure and applied mathematics*, 2(4):331–407, 1949.

- [41] Xiaowen Shan and Xiaoyi He. Discretization of the velocity space in the solution of the boltzmann equation. *Physical Review Letters*, 80(1):65, 1998.
- [42] SS Chikatamarla, SKIV Ansumali, and IV Karlin. Grad's approximation for missing data in lattice boltzmann simulations. *EPL (Europhysics Letters)*, 74(2):215, 2006.

## 5 Supplementary Material: Fluid-kinetic multiscale solver for wall-bounded turbulence

Fluctuations in the near-wall region:

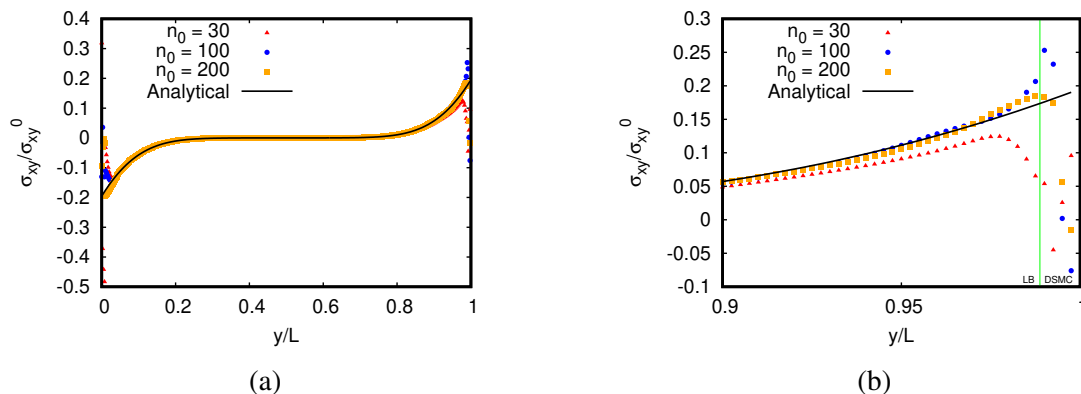


Figure 7: (a) Normalized shear stress profile at  $\bar{t} = 7.49 * 10^{-3}$  for simulations performed using 30, 100 and 200 particles per cell compared against the analytical solution. (b) A magnified version of the near-wall region.

Simulations using 30, 100, and 200 particles per cell were performed in order to assess the effects of number density on the fluctuations in the near-wall stress profile. This information is reported in Figure 7a & 7b, from which it is seen that the standard deviation decreases with increasing  $n_0$ , as also shown in Table 1.

$n_0$	$\sigma_{(\bar{y} \geq 0.9)}$	$n_0$	$\sigma_{(\bar{y} \geq 0.95)}$
30	0.308959	30	0.435186
100	0.176806	100	0.249875
200	0.154661	200	0.218377

Table 1: Standard deviation ( $\sigma$ ) of the shear stress fluctuations with different number of particles per cell, measured for data points  $\bar{y} \geq 0.9$  and  $\bar{y} \geq 0.95$ . Here  $\bar{y} = y/L$  is the nondimensional length.